Mechanical Systems and Signal Processing 166 (2022) 108437

Contents lists available at ScienceDirect

Mechanical Systems and Signal Processing

journal homepage: www.elsevier.com/locate/ymssp

Vibration measurement of a rotating cylindrical structure using subpixel-based edge detection and edge tracking

Aisha Javed [a], Hyeongill Lee [b], Byeongil Kim [c], Youkyung Han [a,*]

[a] Department of Civil Engineering, Seoul National University of Science and Technology, Seoul 01811, Korea
[b] School of Automotive Engineering, Kyungpook National University, Sangju 37224, Korea
[c] School of Mechanical Engineering, Yeungnam University, Gyeongsan 38541, Korea

ARTICLE INFO

Communicated by Javad Baqersad

Keywords:
Vibration detection
Subpixel-based edge detection
Edge tracking
Photogrammetry
Target-less approach

ABSTRACT

Acceleration sensors are commonly used for measuring the vibrations of structures. However, these contact-type sensors cannot be installed in some areas, such as on objects located in hazardous areas. Recently, non-contact-type measurement approaches, including photogrammetry techniques (e.g., point tracking, digital image correlation, and target-less approaches) have been introduced using images obtained from cameras. Nevertheless, photogrammetric approaches, e.g., point tracking and digital image correlation, have the same problem because targets or high-contrast speckle patterns need to be mounted on structures. Instead, the target-less approaches for vibration measurement were developed and tested on static structures like bridges and other civil structures. However, analysts have rarely focused on the rotating axis of cylindrical structures, which is a general component of the rotation-based renewable power generation system. Therefore, in this paper, we introduced a subpixel-based vibration measurement method for a cylindrical rotating structure based on the video images acquired from a non-contact sensor. The frames were magnified, and subpixel-based edges were detected in each frame of the video. Then, using the proposed edge tracking technique, the coordinates of the edges in a region of interest were tracked throughout the video for measuring the vibrations. The proposed edge tracking technique keeps the track of the edge locations in the previous frame as well as the locations in the pixels of the current frame. To show the effectiveness of the proposed method, two simulation datasets and one real dataset were constructed. For the simulation datasets, we generated videos by adding sinusoidal noises together with random noise in an image that contains a static cylindrical object. For the real dataset, a video of a rotating cylindrical object was acquired. The results obtained using the proposed method were compared with the results obtained using the existing multi-interval second-order differential edge detection technique and partial area-based technique. From the simulation datasets, vibrations related to both the single and multiple frequencies were effectively detected by applying the proposed method. The proposed method had the lowest root mean square error (RMSE) calculated with the reference data compared to the existing methods. In the real dataset, we could demonstrate that the proposed method could effectively detect the vibrations on the rotating axis of a cylindrical structure with the exact locations of the edges while removing the non-interest edges or false edges. Moreover, during the frequency analysis, the peaks of the proposed method results were at the same frequency at which the object was rotating. Therefore, the proposed method can be a useful solution to detect the

* Corresponding author at: Department of Civil Engineering, Seoul National University of Science and Technology, Seoul 01811, Korea.
E-mail addresses: javedaisha123@seoultech.ac.kr (A. Javed), hilee@knu.ac.kr (H. Lee), bikim@yu.ac.kr (B. Kim), han602@seoultech.ac.kr (Y. Han).

https://doi.org/10.1016/j.ymssp.2021.108437
Received 5 April 2021; Received in revised form 12 August 2021; Accepted 9 September 2021
Available online 17 September 2021

vibration of rotating structures located in hazardous areas with uneven backgrounds and uneven brightness.

1. Introduction

Nowadays, rotating cylindrical structures are utilized in various industries. The performance of these structures can be affected by factors like loose connections. Therefore, constant monitoring of these structures, which can help in maintaining the efficiency and performance of the structure to its optimal level, is required. To detect faults in rotating structures, vibration measurement is commonly used. It is extensively used to understand the fundamental physics of structures, monitoring their dynamics, and validating and updating the analytical models [1]. In the past few decades, to acquire the highest possible accuracy, various vibration measurement sensors and computer processing techniques have been developed; these techniques focus on the various types of structures (e.g., buildings, bridges, turbines, and airplanes).

To measure the vibrations of a structure, contact-type sensors (e.g., accelerometers or gap sensors) are commonly utilized [1]. However, it is difficult to measure the vibration of a structure in areas where these contact-type sensors cannot be installed, like hazardous areas. Therefore, recently photogrammetry techniques, which are non-contact-type approaches, have been developed and being applied to measure the vibrations of different types of structures [2,3,4,5,6]. Depending on the type of target used, the photogrammetry techniques can be categorized into different approaches, such as point tracking [7], digital image correlation (DIC) [8,9], and target-less approaches [10,11].

The point tracking approach is exploited for testing and identifying the deformation in a structure by using photogrammetric cameras to track and measure the displacement of a series of optical targets mounted on a structure [1]. Analysts have developed different point tracking techniques to detect the vibration of various types of structures (e.g., wind turbines, irregular structures, buildings, bridges, and L-shaped beams) [7,12,13,14,15,16,17,18]. On the other hand, the DIC approach works based on the grayscale variation of continuous patterns. First, high-contrast speckle patterns are applied to the structure, and a series of images are acquired. Then, the subsets of the speckles are created and tracked throughout the whole series of images. Recently, multiple DIC approaches have been introduced for 3D vibration measurement, full-field vibration analysis, shape vibration test, and vibration detection of a rotating disc [19,20,21,22,23,24].

In the past few years, many researchers have showed the advantages of point tracking and DIC photogrammetric algorithms to measure the vibrations of different types of structures. However, a structure needs to be prepared before applying these techniques. To perform a point tracking approach, optical targets need to be mounted on the structure. For conducting the DIC approach, the surface of the structure needs to be prepared with patterns of speckles on it. Therefore, these methods cannot be applied in areas where it is challenging to put the targets or speckles on a structure. Besides, the aforementioned techniques cannot be applied to a rotating cylinder because a camera will only record one side of the structure; when a cylinder rotates, the camera will not be able to track the speckles or patterns on the other side.

Therefore, recently, research scientists have utilized target-less approaches to measure the vibrations of cylindrical structures. The target-less approaches do not need any targets or patterns to find the faults in a structure. To track the vibration of a structure in a region of interest (ROI), analysts have extracted edges or internal features of that structure. For example, an optical flow vector that provided information regarding the direction of vibration in a cable was introduced in [25]. Moreover, for the vibration measurement of static structures like cables, bridges, and traffic signals, various methods using natural textures of a structure, wavelets, edge detections, and mask convolution techniques were introduced [11,25,26,27,28,29].

Among various target-less approaches, the edge detection technique is used more frequently because of its low computational costs and the possibility of extracting the entire length of the structure [30,31,32,33]. The edge detection technique is based on the fact that the dynamics of a rotating or moving structure can be determined by using the boundaries of that structure. Edges are simply detected by looking for the sharp changes in the image brightness. However, conventional edge detection techniques (e.g., Sobel, Prewitt, and Canny edge detection) give approximated integer-type coordinate locations of an edge. To avoid error inheritance in the result and to obtain the actual location of edges, the location needs to be expressed as a real number–type coordinate values. Recently, a multi-interval second-order differential technique has been introduced to address this problem for the real number coordinate location of an edge of a structure [34]. They detected the vibrations of a cylindrical structure introduced by a vibrator. The technique was based on the maximum value and second-largest value in the ROI from the result of the first-order edge detection technique. These two values were then used to detect a real number–type coordinates location of an edge. However, the uneven brightness and background in a video can affect the maximum and second-largest values, which can cause the false coordinate location of an edge and thus disturb a reliable vibration measurement result.

In summary, many researchers have focused on measuring the vibrations of a structure by utilizing edge detection techniques, but they have applied these techniques to either static structures (e.g., bridges, traffic lights, and cylindrical structures like pipes) or tested their algorithms on rotating blades of a wind turbine. Studies have rarely focused on the rotating cylindrical structure, which is a general component in many industrial systems like rotation-based renewable power generation systems. Also, the falsely or closely detected edges in the ROI which can negatively affect the result of vibration measurement were not considered.

Therefore, in this study, we aim to perform vibration analysis on a rotating cylindrical structure by using a subpixel-based edge detection technique together with an edge tracking technique that utilizes frame-to-frame comparison with a pixel-to-pixel comparison of edge locations. The proposed method can effectively detect the vibrations on the rotating axis of a cylindrical structure while

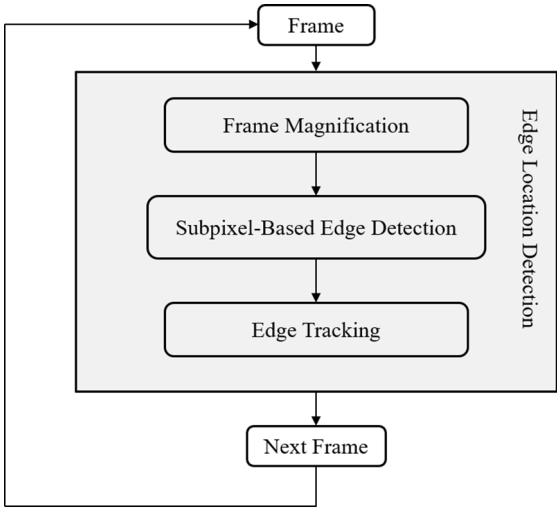

Fig. 1. Flowchart of the proposed vibration estimation method based on edge location detection.

considering and thus removing the falsely detected edges that are caused by an uneven background or uneven brightness in a video. To show the effectiveness of the proposed method, two simulation datasets were prepared by applying periodic noises together with random noise in the image of a static cylindrical object to create the vibration videos of a rotating cylindrical structure. Then, the proposed method was applied to detect the vibrations in the simulation data. Also, a video of a real rotating cylindrical structure was recorded with a commercially available camera, and the proposed method was tested. To conduct the accuracy assessment, the results of the proposed method were compared with the ones generated by the existing multi-interval second-order differential edge detection technique [34] and partial area-based technique [35]. The vibration measurement results were numerically evaluated by calculating the root mean square error (RMSE) with reference data. Moreover, we performed frequency analysis to measure the primarily occurring vibrations including the one related to the rotation speed of the cylindrical structure.

The rest of the paper is organized as follows. The implementation of the proposed method is described in Section 2. In Section 3, the simulation and real data acquired are introduced, after which the results obtained by the proposed method and existing vibration measurement techniques in both datasets are given. Finally, Section 4 outlines the conclusion of the study.

2. Methodology

Fig. 1 shows the flowchart of the proposed vibration estimation method based on edge location detection. The proposed edge detection method was applied to each frame. Then, the detected edge result of each frame was combined along the frame domain to estimate the vibrations on the rotating axis of a cylindrical structure. The proposed method involves three main steps, namely, frame magnification, subpixel-based edge detection, and edge tracking. Each step is explained properly in the following subsections.

2.1. Frame magnification

To measure the vibrations on the rotating axis of the cylinder, the frame was magnified before applying the subpixel-based edge detection technique. Vibration measurement results can be affected by the noises produced in a frame because of the quality of the camera or the uneven background of the frame; this can result in the false detection of edges. Therefore, to avoid such noises impacting negatively on the extraction of edges from the object, and to detect the exact location of the edges on the subpixel level, each frame in the video was first magnified by using the bicubic interpolation that could reduces the artifacts including blurring and aliasing in a magnified image unlike other interpolation techniques [36].

2.2. Subpixel-Based edge detection

The traditional edge detection technique gives approximated integer-type location of an edge. However, using such edge detection techniques to measure vibrations may result in losing information related to the vibrations of a structure. In a study, Son et al. [34] addressed this problem by introducing a multi-interval second-order differential technique to estimate the real number–type coordinate location of an edge of a structure. They utilized the first-order derivative and showed it as a Gaussian distribution to determine the maximum and second-largest coordinate values for a zero-crossing point. Then, these two values were placed in the result of the mean of the multi-interval second-order differential technique, and a straight-line equation that passes through two points was used to detect a real number–type edge location in an ROI. However, the aforementioned technique is based on the maximum and second-largest values in the Gaussian distribution of the first-order derivative. These values can be affected by the uneven background of

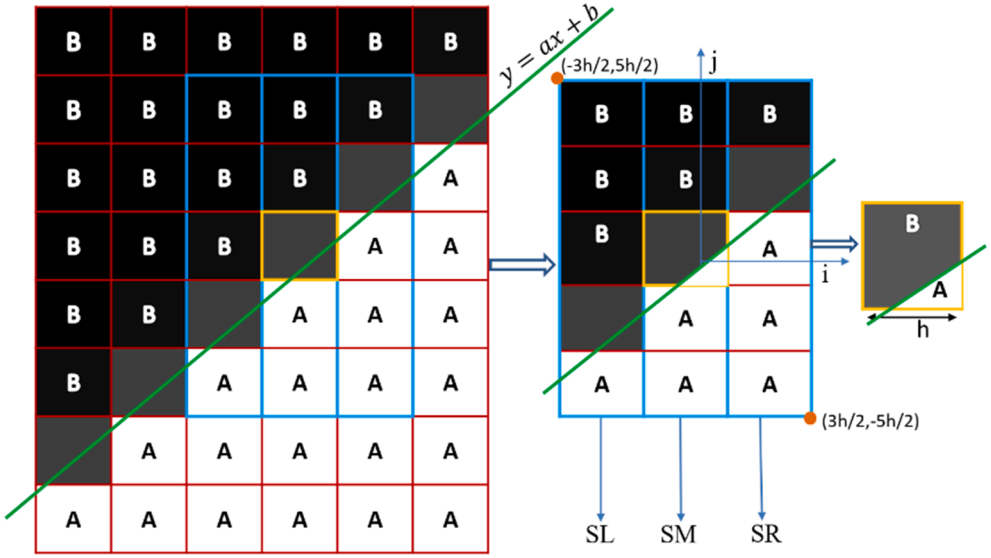

Fig. 2. Region/pixel divided into two areas by an edge represented by a straight line.

an object or the frame quality or the brightness in the ROI; consequently, these values can be extracted outside the edges of a structure, which can result in false real number–type edge locations.

The subpixel-based edge detection technique introduced by Trujillo-Pino et al. [35] gives the exact location of an edge relative to the object of interest because instead of analyzing the maximum gradient or zero crossings on a supposedly continuous signal that describes the image, this method assumes a certain discontinuity in the signal where the edge exists. It attempts to accurately locate this edge by assuming a partial area effect produced by the acquisition process in the image values. In simple words, this technique is based on the fact that an edge divides a region or a pixel into two areas having different intensity values. Due to its high reliability for detecting the edges of a structure, we applied the subpixel-based edge detection technique [35].

Before applying the subpixel-based edge detection, the gradient of an image was computed by using traditional derivative masks, e.g., partial derivatives. Then, a threshold (T_e) was selected to detect the edge pixels in a frame. After detecting the edge pixels in a frame, a straight line that fits the dominant edge pixels was estimated to obtain the exact location of each edge at a specific position at the subpixel level. This was done by calculating the intensity ratios on both sides of an edge in each frame. Let us assume that an edge of an object is a straight line as expressed by the following equation [35]:

$$y = ax + b \tag{1}$$

where a and b are the coefficients of a straight line.

The considered straight line passing through pixels divides each pixel into two regions, which are above and below the line in a pixel/region, and have intensity values of A and B, respectively. Assuming that a, b , A, and, B are known, then the pixel values will follow the fact that the gray colored pixels between the regions A and B (as shown in Fig. 2) may have an intermediate value between A and B [35]. The above statement can be expressed as follows.

$$P(i,j) = B + \frac{A-B}{h^2}E(i,j) \tag{2}$$

where $P(i,j)$ is a pixel value at the position (i,j) which could have an intermediate value between A and B, h denotes the length of a pixel side, and $E(i,j)$ is the area under the edge line inside the pixel coordinate (i,j).

For the sake of simplicity, a 5×3 window centered on the pixel (i,j) is considered as shown in Fig. 2. The sum of the pixel values in the left (S_L), middle (S_M), and right (S_R) columns can be calculated by using the following equations:

$$\begin{aligned} S_L &= \sum_{n=j-2}^{j+2} P(i-1,n) = 5B + \frac{A-B}{h^2}E_L \\ S_M &= \sum_{n=j-2}^{j+2} P(i,n) = 5B + \frac{A-B}{h^2}E_M \\ S_R &= \sum_{n=j-2}^{j+2} P(i+1,n) = 5B + \frac{A-B}{h^2}E_R \end{aligned} \tag{3}$$

here E_L, E_M, and E_R denotes the areas under the edge line inside the left, middle, and right columns, respectively. These areas can be derived by using equation (4).

$$E_L = \int_{-3h/2}^{-h/2}\left(b + ax + \frac{5h}{2}\right)dx = bh - ah^2 + \frac{5}{2}h^2$$

$$E_L = \int_{-h/2}^{h/2}\left(b + ax + \frac{5h}{2}\right)dx = bh + \frac{5}{2}h^2 \tag{4}$$

$$E_R = \int_{h/2}^{3h/2}\left(b + ax + \frac{5h}{2}\right)dx = bh + ah^2 + \frac{5}{2}h^2$$

By utilizing the expression forS_M, the coefficient b can be obtained by equation (5).

$$b = \frac{2S_M - 5(A+B)}{2(A-B)}h \tag{5}$$

To estimate$a$, the expressions for S_L and S_R of 5 × 3 window can be utilized as follows:

$$a = \frac{S_R - S_L}{2(A-B)} \tag{6}$$

To estimate the intensity values of area A and B, three pixels on the opposite corner of the window from the centered pixel can be used as follows:

$$\begin{aligned} A &= \frac{1}{3}\left(P(i,j-2) + P(i+1,j-2) + P(i+1,j-1)\right) \\ B &= \frac{1}{3}\left(P(i+1,j+1) + P(i+1,j+2) + P(i,j+2)\right) \end{aligned} \tag{7}$$

To find the subpixel position of an edge, the vertical distance from the center of a pixel to the edge is calculated as (0,b).

To perform second-order edge detection, the edge can be represented by a second-order curve $y = ax^2 + bx + c$. If $x = 0$, the slope of the second-order curve ranges between 0 and 1. In addition, to find the subpixel position of the edge in a pixel, we utilized the same window size as that used for the first-order subpixel-based edge detection. The values under the edge line in the three columns E_L, E_M, and $E_R$are given by the following equations:

$$E_L = \int_{-3h/2}^{-h/2}(c + bx + ax^2 + \frac{5h}{2})dx = ch - bh^2 + \frac{13}{12}ah^3 + \frac{5}{2}h^2$$

$$E_M = \int_{-h/2}^{-h/2}(c + bx + ax^2 + \frac{5h}{2})dx = ch + \frac{1}{2}ah^3 + \frac{5}{2}h^2 \tag{8}$$

$$E_R = \int_{h/2}^{3h/2}(c + bx + ax^2 + \frac{5h}{2})dx = ch + bh^2 + \frac{13}{12}ah^3 + \frac{5}{2}h^2$$

By utilizing the sum of the three columns similar to first-order subpixel-based edge detection, coefficients a, b, and c were calculated by using equation (9), while considering $h = 1$.

$$a = \frac{S_L + S_R - 2S_M}{2(A-B)}$$

$$b = \frac{S_R - S_L}{2(A-B)} \tag{9}$$

$$c = \frac{2S_M - 5(A+B)}{2(A-B)} - \frac{1}{12}b$$

The subpixel position of an edge was determined the same way as first-order subpixel-based edge detection by using the coordinates (0,c). By putting $a = 0$ in the second-order curve, first-order edge detection can be carried out. The aforementioned techniques find the edge in the y-direction. To find the edge in the x-direction, the window must be rotated as 3 × 5 and the equation for the subpixel position should be measured horizontally from the center of the pixel to the edge; its coordinates are thus $(c, 0)$.

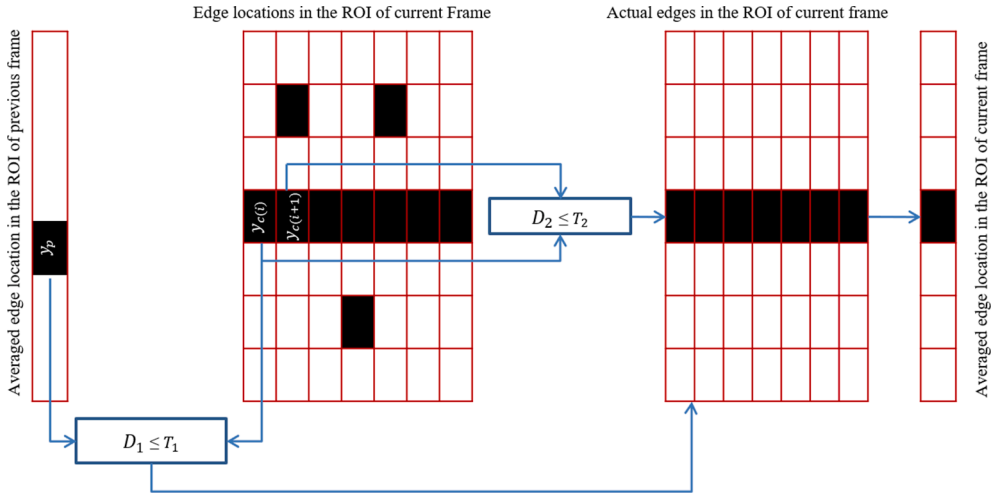

Fig. 3. Proposed edge tracking technique.

2.3. Edge tracking

Even after magnifying a frame, the vibration measurement technique can still be affected by false edges in the ROI of some frames caused by the acquisition condition of video data. Therefore, to track the actual location of the edges of an object in ROI throughout the video and to remove the false edges from ROI, the edge tracking technique is proposed. The proposed edge tracking process determines the subpixel position of an edge in the pixel i in the current frame by comparing this position with the averaged subpixel-based edge locations in the ROI of the previous frame and with the subpixel position of an edge in the $i+1$ pixel (i.e., the next pixel in the current frame). To do so, the first frame is treated as a reference frame, and the ROI is selected in the first frame after the edges are detected. Then, the subpixel location of an edge in the current pixel was compared with the subpixel location of an edge in the next pixel. If the difference between the subpixel location of the edges in the current pixel and the next pixel is less than or equal to a specific threshold (T_2), then the current edge will be treated as the actual edge of the object of interest. After effectively detecting the locations of the actual edges of an object in the first frame, these values were averaged. Then, the next frame was treated as the current frame, and the edges were detected. Subsequently, the subpixel locations of each edge in the ROI of the current frame were subtracted from the averaged subpixel locations of the edges in the previous frame. Then, another threshold (T_1) was selected, and the result of the difference between the current pixel's edge location and the previous frame was compared with T_1. Also, similar to the first frame of a video, the subpixel location of an edge in the current pixel was compared with the subpixel location of an edge in the next pixel. The aforementioned method can be expressed as equation (10).

$$\begin{aligned} D_1 &= y_{c(i)} - y_p \\ D_2 &= y_{c(i)} - y_{c(i+1)} \end{aligned} \tag{10}$$

where $y_{c(i)}$ denotes the edge location in the y-direction in a pixel i in the current frame, and y_p is the averaged edge location in the y-direction in the ROI of the previous frame. $y_{c(i+1)}$ is the edge location in the y-direction in a pixel $i+1$. D_1 is the difference between the edge location in a pixel i in ROI of the current frame and averaged edge locations in ROI of the previous frame. While D_2 is the difference between the edge location in a pixel i and $i+1$ in ROI of the current frame.

The difference between the edges' locations in the ROI of the previous frame and the current frame will be significant compared to the difference between those of the current frame. Therefore, two thresholds T_1 and T_2, which are related to a pixel-to-previous frame difference (i.e., edge location in a pixel of the current frame with the average of edge locations in the ROI of the previous frame) and a pixel-to-pixel difference, respectively, were selected by considering the relationship, i.e., T_1 is larger than T_2. After obtaining D_1 and D_2, they were compared with T_1 and T_2, respectively. If D_1 is less than or equal to T_1, as well as if D_2 is less than or equal to T_2, then the current edge location in a pixel will belong to the edge of an object. Otherwise, it will be treated as a false edge that does not belong to the object and thus removed from the ROI. After effectively detecting the true edges of an object in the ROI of the current frame, the edges are then averaged and the same process is repeated for the next frame. The overall process is described in Fig. 3.

The aforementioned technique can effectively remove the false edges that do not belong to the object of interest because of the low quality of a frame. By applying the proposed method to each frame and comparing the edges by using the previous frame information and the next pixel's information in ROI, the vibration of an object can be effectively detected and tracked throughout the video with less amount of noise.

3. Experiment results

To show the effectiveness of the proposed method, two simulation datasets and one real dataset were acquired. While applying the

Fig. 4. An image used to create the simulation data.

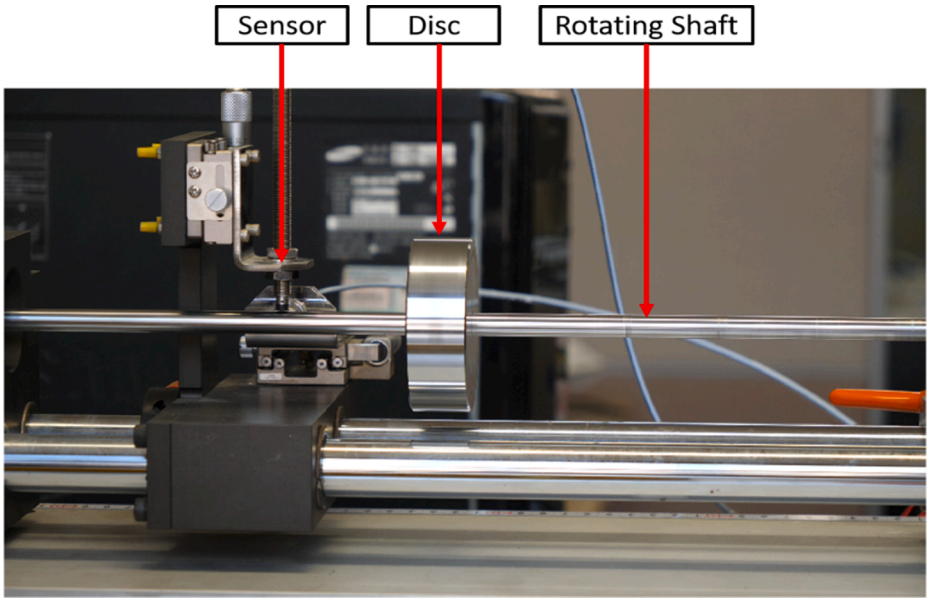

Fig. 5. A frame from the video of a real data.

proposed method, first, a frame was magnified by setting an interpolation ratio. Then, the gradient of the frame was computed to detect the subpixel-level edge locations. Then, the ROI was selected around the rotating axis of an object, and the edges relating to the object boundary were detected and tracked throughout the video frames. While applying the proposed edge tracking technique, thresholds T_1 and T_2 were manually selected. The selection was based on the fact that the pixel-to-previous frame difference will be greater than or equal to one pixel, while the pixel-to-pixel difference will always be less than one pixel. Therefore, in this study, certain thresholds for these two comparisons were applied and the ones with better results were selected. The results obtained from both the simulation and real data were compared with the data obtained from the multi-interval second-order differential technique [34] and the partial area-based edge detection technique [35].

3.1. Data acquisition

To apply the proposed method two datasets were used: simulation dataset and real dataset. Datasets acquisition is explained below.

3.1.1. Simulation data preparation

Usually, a rotating cylinder shows wave variations similar to a sinusoidal wave. Therefore, to create vibrations similar to a real rotating cylindrical structure, we created a video of a cylindrical object with sinusoidal distortions added in the vertical direction at each frame. However, sinusoidal distortions could be easily predicted and detected. Therefore, together with sinusoidal distortions, random noise was also added to each frame to show the effectiveness of the proposed method. An image having a cylindrical rectangular object of 100 × 800 pixels with a clear background was used to generate the simulation video data, as shown in Fig. 4.

To create frames, the original image shown in Fig. 4 was considered as the first frame. Then, the remaining frames were generated by adding sinusoidal distortions and a random noise while considering the frame numbers. The above statement can be expressed as follows:

$$y_i = a \times sin(\frac{f_i}{f_c} \times \pi \times p_1) + b \times cos(\frac{f_i}{f_c} \times \pi \times p_2) + r \tag{11}$$

where a, b, p_1, andp_2 denote the parameters with respect to the amplitudes and periods of the sinusoidal distortions, and r is a normally distributed random noise that has an average of 0 and a standard deviation of 1. In addition, f_i is the number of the i-th frame to be added ($i = 1, \cdots, n$), n is the total number of frames to be created, and f_c is half of the total number of frames (i.e., $c = n/2$); y_i is the added noise amount in the vertical direction of the i-th frame. Based on the process of the simulation data preparation, two types of simulation datasets were prepared: the first one having a single frequency, and the second one having multiple frequencies,

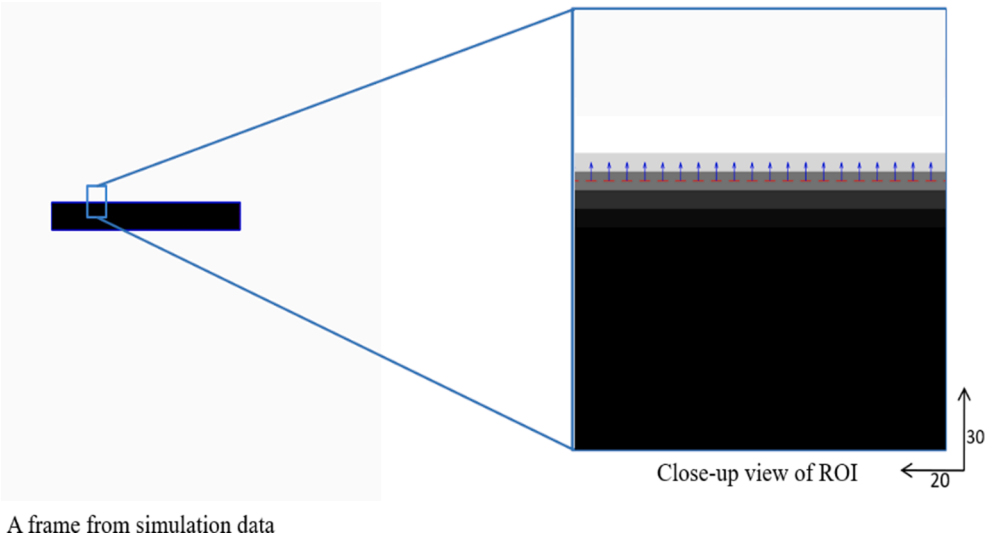

Fig. 6. A close-up view of the ROI selected around the upper edge of the cylindrical object in the simulation data. The red lines are subpixel positions of the edges, and the blue arrows are their normal vectors. (For interpretation of the references to colour in this figure legend, the reader is referred to the web version of this article.)

respectively.

To create the first simulation data with a single frequency, a single sinusoidal distortion was added together with a random noise by setting the parameter b to 0. Moreover, the parameter a was set to 2 and p_1 was selected as 30, and a total of 600 frames (i.e., $n = 600$) were generated from the original image. After generating the noise by using Equation (11), it was added to the y-axis of the original image, and a new frame was created. The frames were added to a video at the rate of 59.94 frames per second.

In the case of the second simulation data, a more complex noise was added based on the fact that vibrations in a real rotating cylinder occur at multiple frequencies because of radial and tilt error motions of a shaft [37], e.g., circular characteristics of the shaft such as trilobe, eccentricity, ovality, and squareness. To do so, together with a single sinusoidal noise and random noise in the first simulation data, another sinusoidal noise was added by setting the parameters b and p_2 to 3 and 15, respectively, while other parameters were left unchanged. By applying the simulation data preparation, we could create sinusoidal movements like cylinder vibrations in the vertical direction.

3.1.2. Real data

To test the proposed method on real data, a video of a rotating cylindrical structure was acquired by using Panasonic Lumix DC-GH5, a commercially available digital camera. The object rotated at the rate of 300 rotations per minute, which means the object rotated 5 times in one second, that is, 5 rotations per second (rps). The video was of 31 sec duration with a frame size of 1,920 × 1,080. The distance from the camera to the structure was approximately 135 cm. To remove the movements generated at the start and end of the video, the frames at the start and the end were removed, and experiments were carried out on 12.7 sec of the video. To show the effectiveness of each step completely in the proposed method, the video was recorded with an uneven background having non-interest objects along with the rotating cylindrical structure, as shown in Fig. 5.

3.2. Experiments on simulation data

The simulation data preparation given in Section 3.1.1 was used to verify the proposed method using qualitative and quantitative assessments. The proposed method was applied to the video generated for the first simulation data. To this end, first, the frame size was magnified to twice the size of the original frame (i.e., from 2000 × 2000 to 4000 × 4000) by selecting the interpolation ratio as 2. Then, the magnified frame was converted from a red–green–blue image to a gray image. After obtaining the gray image, the gradient was computed and the threshold T_e was selected for finding the edge pixels. In this experiment, we determined the pixels belonging to the edge of an object by selecting the $T_e$values as 11. We selected an ROI having a size of 30 × 20 pixels in the magnified frame (i.e., 15 × 10 pixels in the original frame) around the upper rotating axis of the object. Fig. 6 shows a close-up view of the selected ROI with the detected edges in the magnified frame. The red lines are the positions of the edges, and the blue arrows are their normal vectors. Fig. 6 shows that the edges were detected on a subpixel level. After the edges located in the ROI of the first frame were extracted, their locations were averaged in order to be utilized as additional information to detect edges in the next frame.

The same edge detection approach that was applied for the first frame was applied in the second frame. Then, the location of an edge in each pixel in the ROI of the second frame was compared with the averaged location of the previous frame. This location was also compared with the location of an edge in the next pixel in the x-direction by applying the proposed edge tracking technique. To make these two comparisons, T_1 and T_2 were selected as described in the methodology. T_1 tends to be higher than T_2because the edge

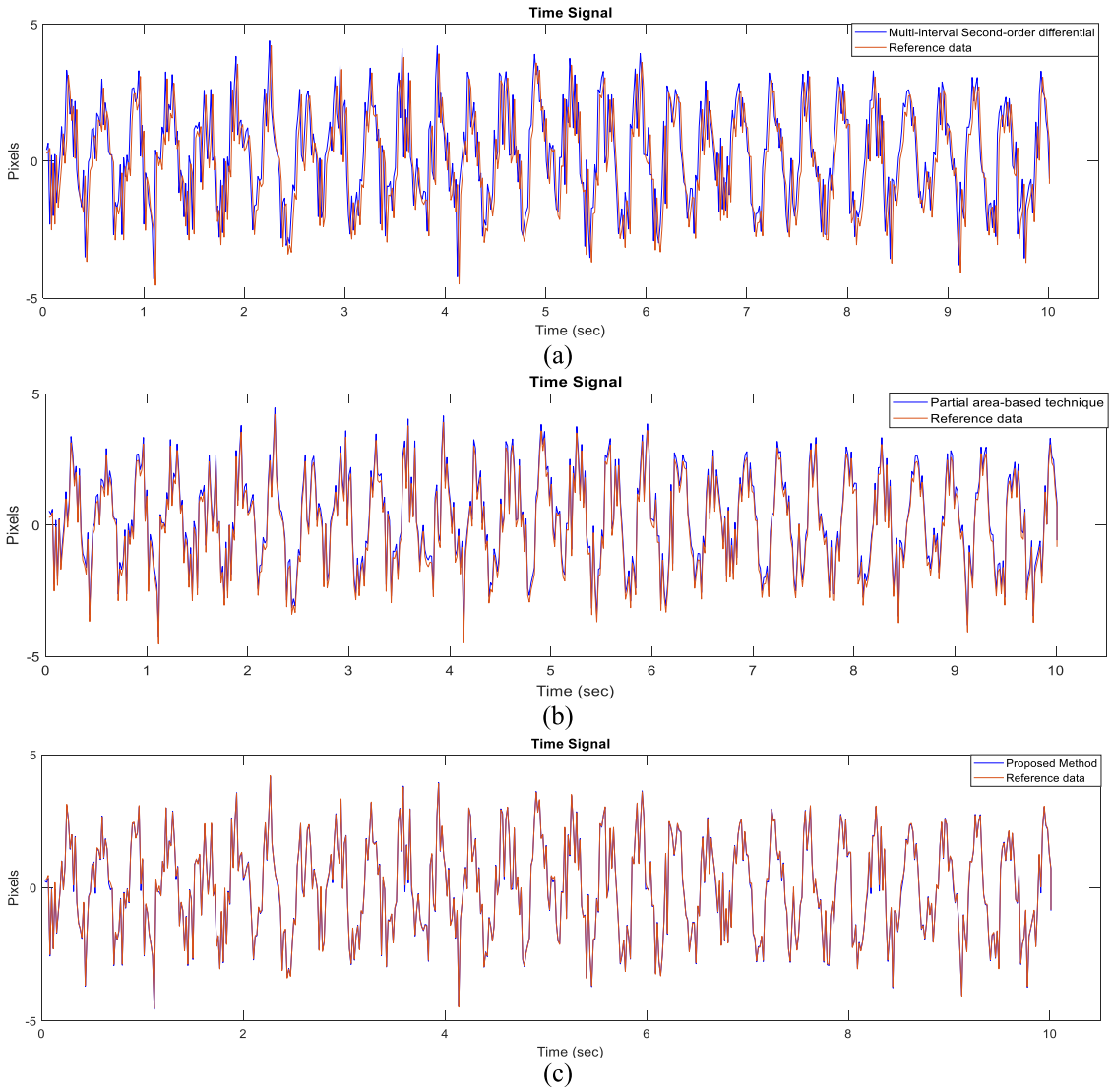

Fig. 7. Vibration measurement results in the first simulation data: (a) Multi-interval second-order differential technique, (b) Partial area-based technique, and (c) Proposed method.

location of the frame-to-frame difference will be more significant than that of the pixel-to-pixel difference. Therefore, to select the appropriate values for T_1 and T_2, we analyzed the results after applying multiple values of T_1 and T_2; the final threshold values were selected as 9.5 and 0.6 for T_1 and T_2, respectively. After extracting the edge location in the current frame, the values were averaged, and then the same process was repeated for the next frame. By doing this, the vibrations of the simulation data for the whole video frames could be detected.

To conduct the accuracy assessment of the proposed method, the result of Eq. (11) in the first simulation data preparation was recorded throughout the video and used as reference data. These results were added with the column matrix of the original image when the simulation data was made; therefore, it resulted in the movement of the static cylindrical object. Fig. 7 (a), Fig. 7 (b), and Fig. 7 (c) show the reference data and the vibration measurement results obtained by using the multi-interval second-order differential technique, the partial area-based technique, and the proposed method, respectively.

From Fig. 7 (a) it can be seen that by using the multi-interval second-order differential technique, the pattern of the vibration is detected properly. However, as discussed before, this method highly depends on the maximum and the second-largest values in the first-order differential results. If there are close edges that are not from the object in the ROI or if the background is uneven, the edge will highly be detected in the wrong location. This aspect was shown in the graph that the vibration pattern estimated by the multi-interval second-order differential technique seems different compared with the reference data. A similar result was achieved by the partial area-based technique as shown in Fig. 7(b) due to the impact of detecting non-interest edges in the ROI. While from Fig. 7(c) it can be seen that the vibration is detected properly by the proposed method in comparison to the reference data as well as the compared

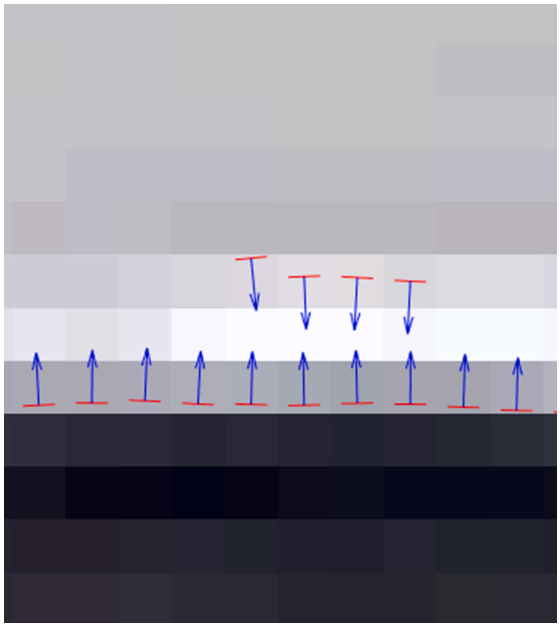

Fig. 8. An example of falsely detected edges in the ROI of simulation data.

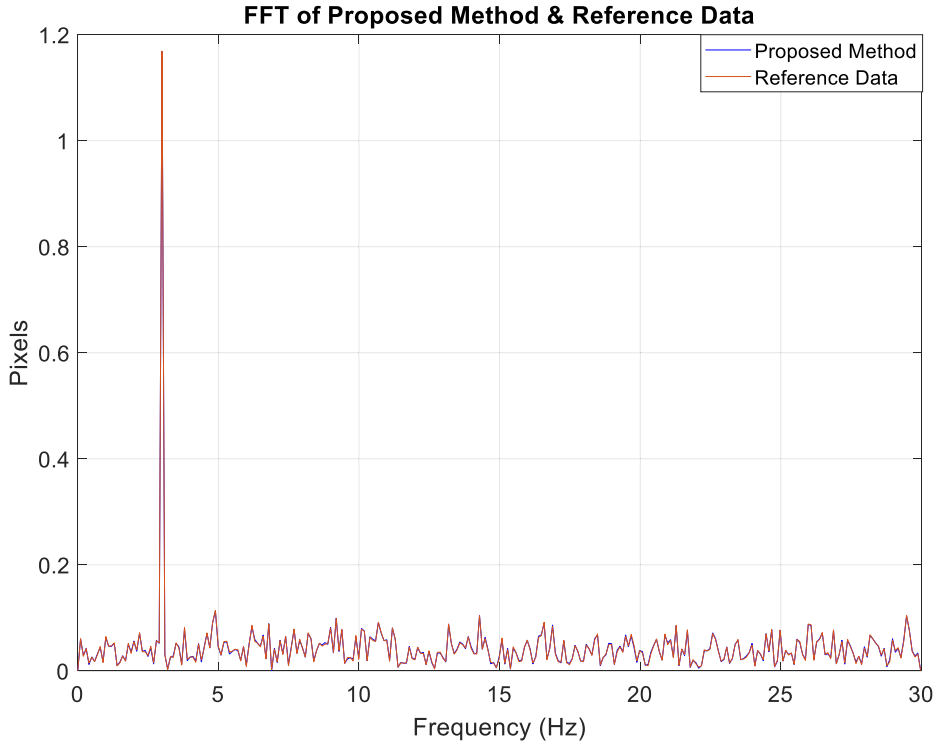

Fig. 9. Frequency analysis of vibration estimated by the proposed method.

vibration measurement techniques. In addition, the proposed edge tracking technique effectively removed false edges by tracking only the edges relating to the object of interest using the averaged edge location of the previous frame and adjacent edge location information of the current frame. Fig. 8 shows an example of false edges in ROI resulting in the poor detection of the edge location when applying the multi-interval second-order differential technique and the partial area-based technique.

To quantitatively confirm the comparison results shown in Fig. 7, we calculated the RMSEs between the reference data and the

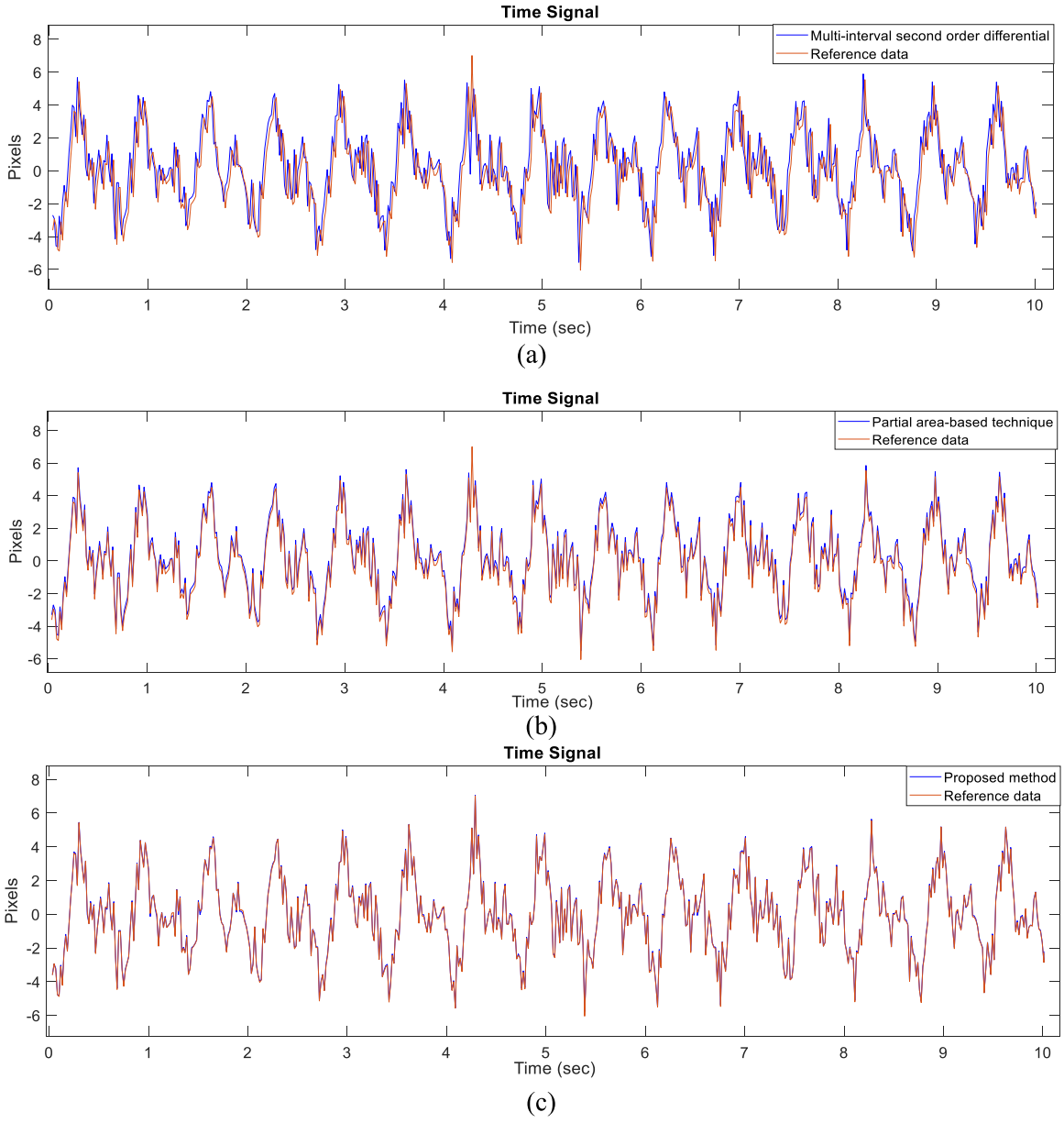

Fig. 10. Vibration measurement results in the second simulation data: (a) Multi-interval second-order differential technique, (b) Partial area-based technique, and (c) Proposed method.

measured vibration results. The RMSE between the reference data and the proposed method was 0.0655, which was the lowest. The RMSE between the reference data and partial area-based edge detection result was 0.2357, and the RMSE between the reference data and the multi-interval second-order differential result was 1.4817.

Frequency analysis in the vibration measurement provides information about the rotation speed of a structure. The frequency analysis results of the proposed method and the reference data are shown in Fig. 9. Clearly, the peak regions and other regions of the proposed method coincided with the reference data. In addition, in the frequency analysis results, the highest peak of both the reference data and the proposed method are at 3 Hz, which is the same as the rotation speed of the simulation data (i.e., 3 rps). We created 30 periods in 600 frames, which is approximately 10 sec of simulation data video; this implies that the object rotated at a speed of 3 rps. Besides, the amplitude of both signals in the frequency analysis is almost the same.

After detecting the vibration in the first simulation data, the second simulation data, adding more complex noises, was utilized to apply the proposed method, and the result was compared with the reference data and other existing techniques. The results are presented in Fig. 10. It can be seen that the graph of the proposed method is much similar to the reference data compared to other existing techniques. Also, at some time intervals, the existing techniques did not show any peak. To clearly show the results mentioned

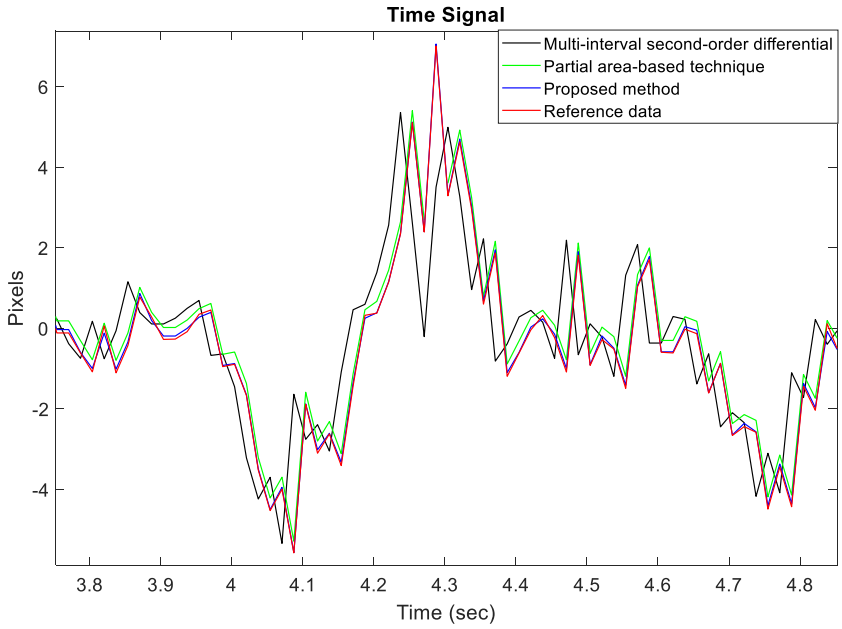

Fig. 11. A close-up view of all the vibration measurement results and reference data.

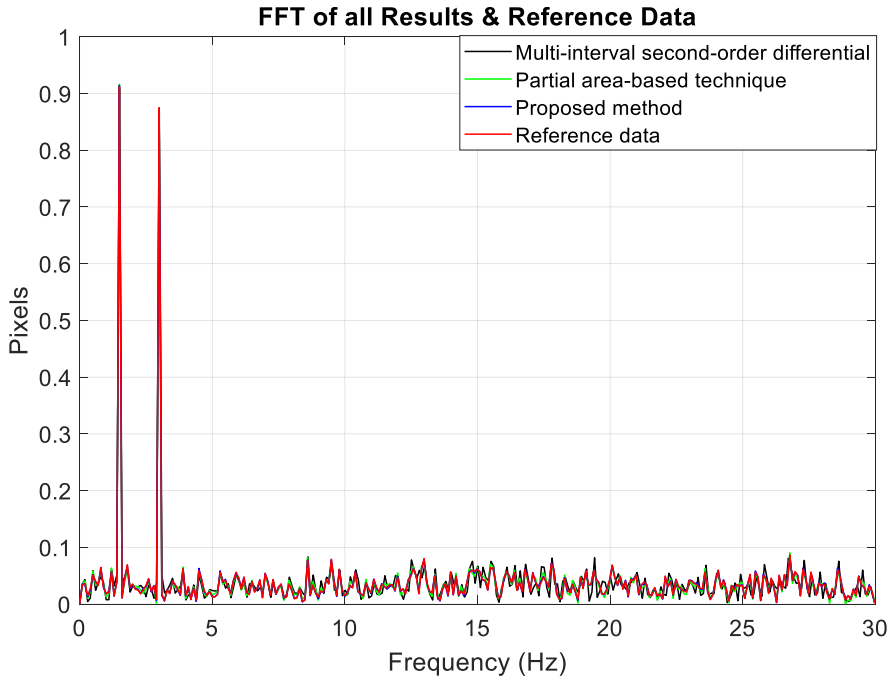

Fig. 12. Frequency analysis of all the vibration measurement results.

above, a close-up view of all the results and the reference data from 3.8 sec to 4.8 sec of the time interval is provided in Fig. 11. As one can see from the figure, the proposed method effectively detected the vibration with the exact location of edges by showing that the graph of the proposed method and reference data (i.e., blue and red graphs in Fig. 11) are much similar compared to other results.

In addition, it can be seen from Fig. 10 that there are two reoccurring patterns of periodic peaks throughout the graphs. One has a higher amplitude (i.e., peaks with an amplitude around 6 pixels) and another one has a lower amplitude (i.e., peaks with an amplitude around 2 pixels). This implies that the cylinder vibrated at two different frequencies. This is because we added two sinusoidal distortions with different periods while making the second simulation data. To effectively show this aspect, frequency analysis was

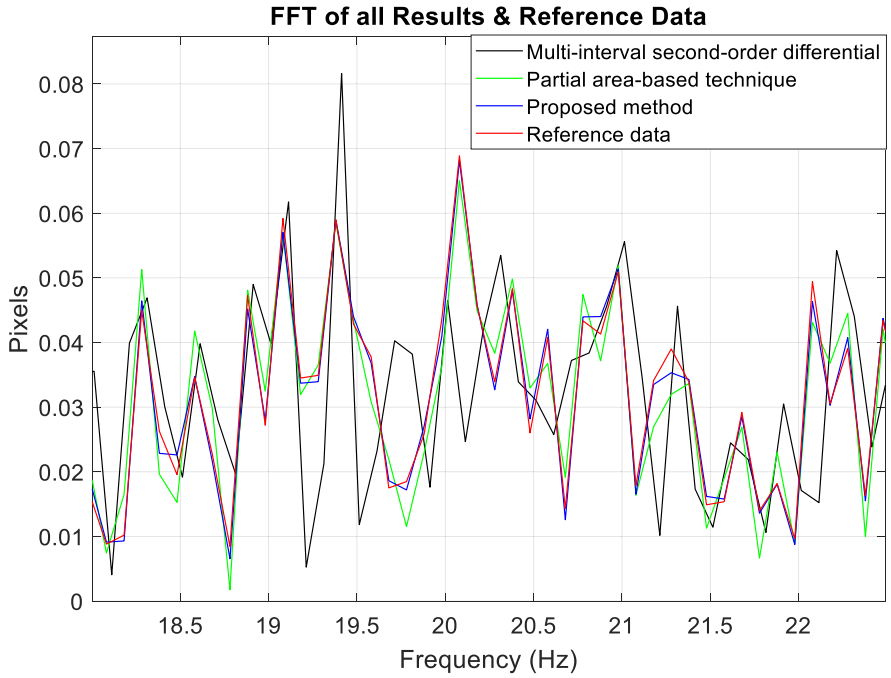

Fig. 13. A close-up view of the frequency analysis of all the vibration measurement results.

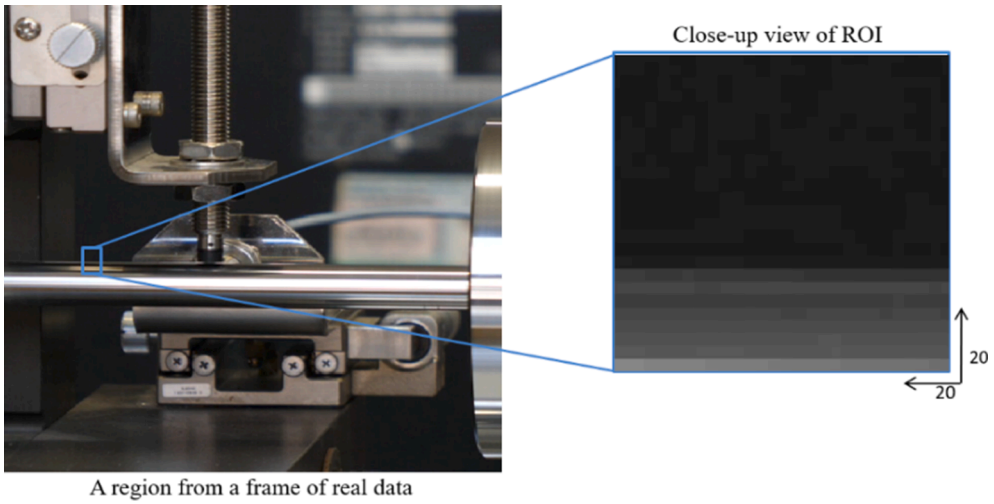

Fig. 14. ROI selected around the upper edge of the cylindrical object in real data.

performed on all the results and provided in Fig. 12. The aforementioned aspect was proved by the frequency analysis of the vibration estimated by all the vibration measurement techniques, which shows two peaks at different frequencies of 1.5 Hz and 3 Hz, similar to the periods of two sinusoidal functions when converted to frequencies. Also, in Fig. 13, a close-up view of the frequency analysis results, shows that the frequency analysis signal of the proposed method has coincided effectively with the reference data, compared to the signals of existing techniques. Moreover, RMSE was calculated between the reference data and all the estimated vibration measurement results to numerically evaluate their performances. The RMSE between the reference data and the proposed method was the lowest with a value of 0.0720, while the RMSE between the reference data and existing multi-interval second-order differential and partial area-based techniques was 1.5697 and 0.3305, respectively.

3.3. Experiments on real data

The vibration measurement was further performed on real data to test its applicability on the real rotating object. As compared with

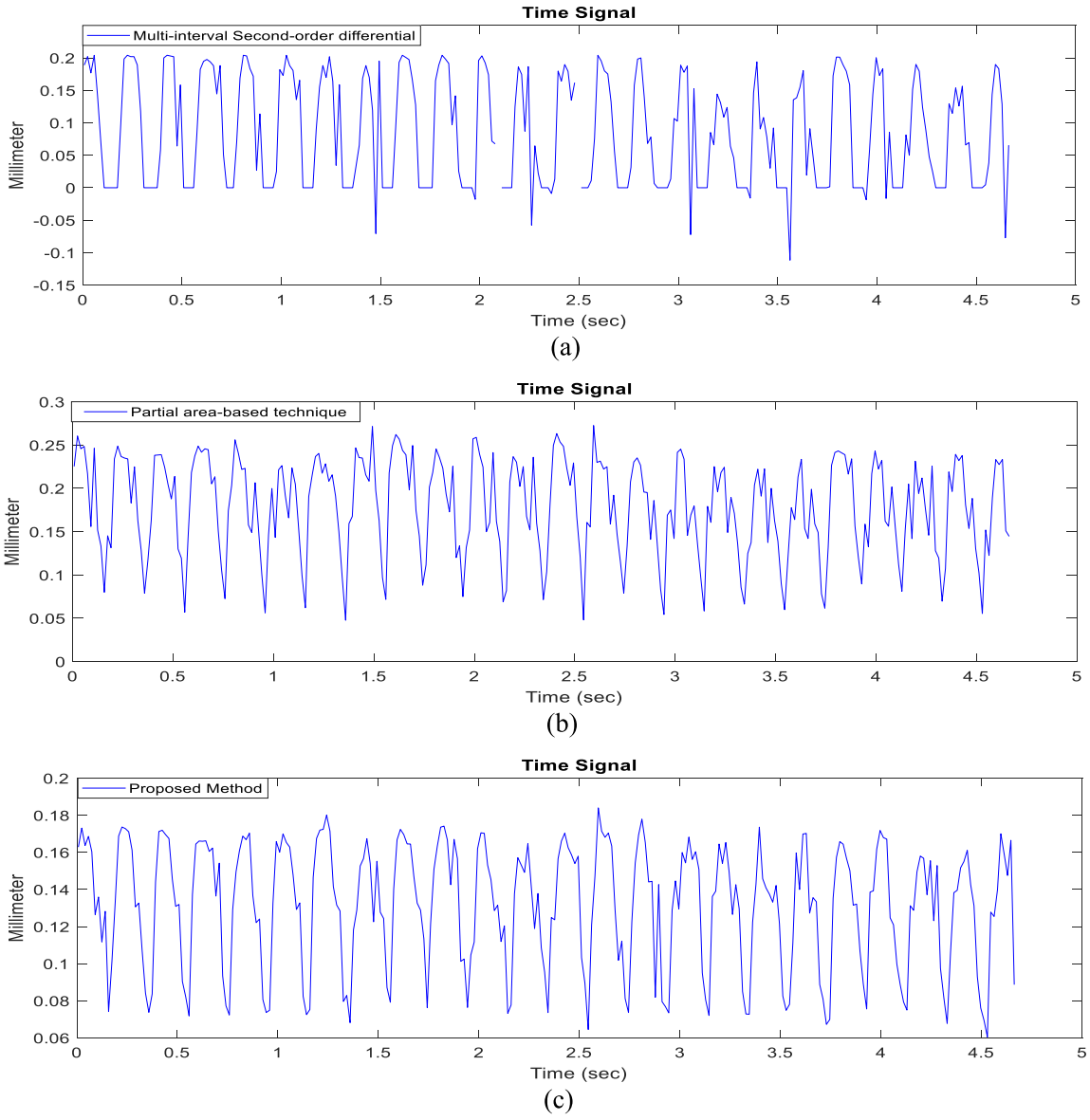

Fig. 15. Vibrations detected in real data: (a) Multi-interval second-order differential technique, (b) Partial area-based technique, and (c) Proposed method.

the simulation data, the background in the video was uneven, and various objects were located close to the rotating object. Consequently, a smaller interpolation ratio would not help to effectively remove the close edges caused by the non-interest objects in the ROI. Therefore, a frame was magnified to three times the size of an original frame. The size of the original frame was increased from 1920×1080 to 5760×3240. Fig. 14 shows a close-up view of the selected ROI. To determine the edge pixels in the magnified frame, a small value was selected for T_e (i.e., $T_e = 5$) because the difference between the brightness values of the object and the background in the ROI was small. Then, the proposed edge detection was applied by taking the ROI size as 20×20 pixels. During the proposed edge tracking technique, T_1 and T_2 were selected as 3 and 0.6, respectively.

The actual diameter of the rotating object was 10 mm, and its size corresponded to 49 pixels in a frame. Using the ratio between the units, we can convert the unit of the vibration measurement result from pixels to millimeters. Fig. 15(a), Fig. 15(b), and Fig. 15(c) show the results obtained by the multi-interval second-order differential technique, the partial area-based edge detection technique, and the proposed method, respectively.

From the graph shown in Fig. 15(a), we can see that the multi-interval second-order differential technique did not detect any edges in ROI at some frames including 2.3 sec as well as 2.5 sec. In addition, this method is highly dependent on the brightness values of the structure and background; therefore, in some frames (e.g., frames located around 1.5 sec, 2.35 sec, 3.1 sec, and 3.6. sec) the location of

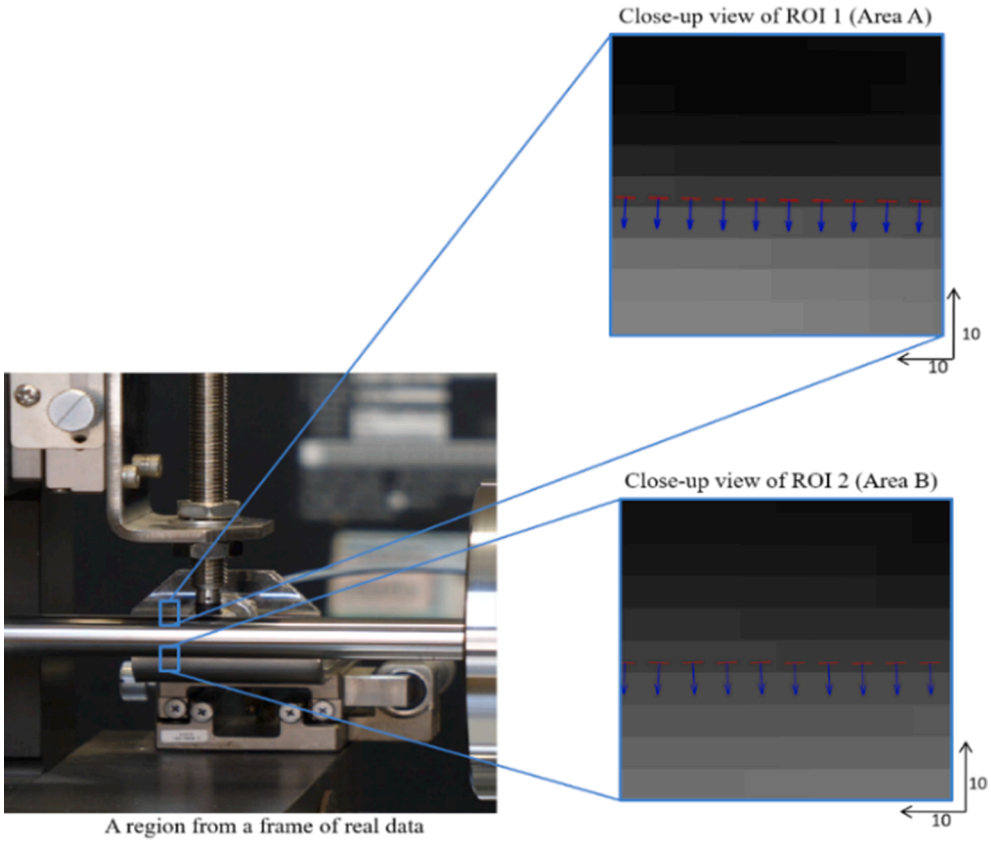

Fig. 16. ROI selected around the upper edge (Area A) and the lower edge (Area B) of the rotating cylindrical object in real data.

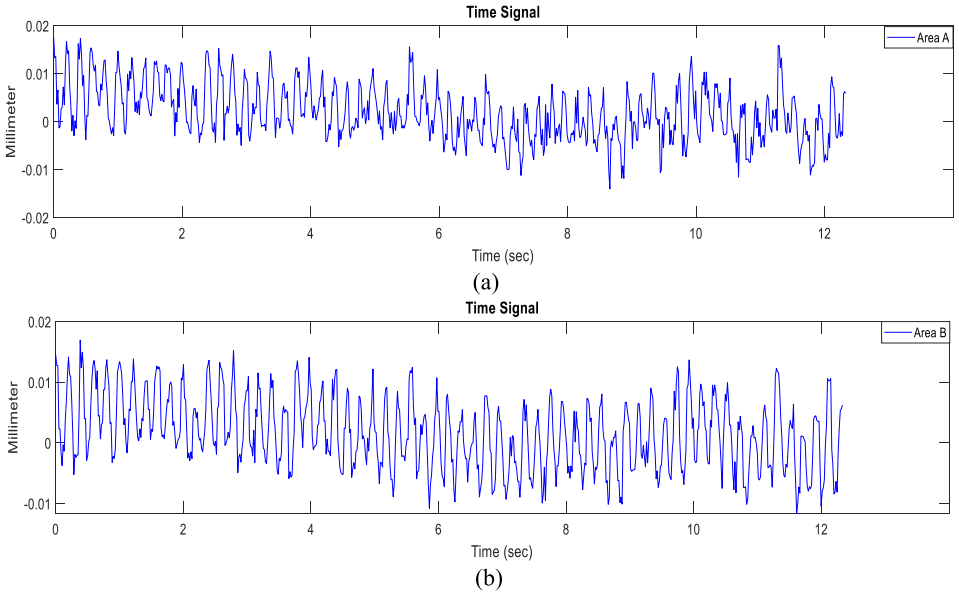

Fig. 17. Vibrations detected in real data by the proposed method: (a) Area A, and (b) Area B.

the edges in ROI were wrongly detected. Therefore, at the aforementioned time intervals, the vibration signal was immediately reduced, and the peaks were shown outside the amplitude of the overall signal. At the down peak of the graph, the amplitude of the signal is constant for 3 to 4 frames, periodically, in other words, the graph did not show any movements at each down peak for about 3

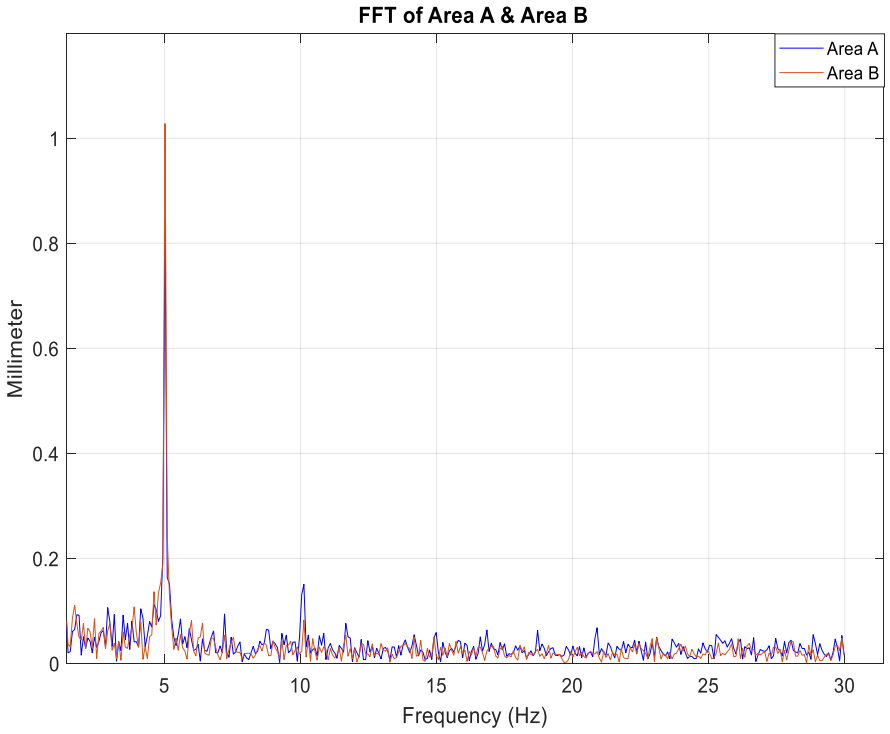

Fig. 18. Frequency analysis of the results obtained in Area A and Area B.

to 4 frames whereas the object of interest was rotating constantly. Besides, the amplitude of the vibration signals in Fig. 15(a) and Fig. 15(b) are different from the signal detected by the proposed method (i.e., Fig. 15(c)) because of the false edges or close edges of non-interest objects in the ROI as discussed in experiments on simulation data. Overall, as compared with the existing methods, the proposed method effectively detected the vibration of the rotating cylinder-shaped object. The proposed method showed that the location of edges in the ROI is continuously changing with time. Furthermore, the peaks of the vibration signal in the graph have almost the same amplitude, and the vibration signal is smoother than the signal detected by the partial area-based edge detection technique.

To show the effectiveness of the proposed method by checking the vibration pattern of the upper edge and the lower edge of the rotating object, we applied the proposed method in the areas where it was difficult to differentiate between the background and the rotating object. The interpolation ratio in the frame magnification process was set to 5; T_e was set to 2, whereas T_1 and T_2were left as before. After the edge detection process, two ROIs of 10×10 pixels were selected around the upper edge (area A) and the lower edge (area B) of the object, as shown in Fig. 16. From a region of the frame, it is clear that the rotating object and the background have almost similar spectral characteristics.

Then, the edge tracking technique was applied, and the vibrations were detected. The vibrations measured in area A and area B for 12.7 sec of the video are shown in Fig. 17(a) and Fig. 17(b), respectively.

From Fig. 17, it is clear that the proposed method detected the vibrations in both areas with almost similar patterns because of the frame magnification and subpixel-based edge detection; however, the amplitudes of both signals were different from each other during some time intervals. Even though the proposed method detected the edges in the ROI, because of the similar spectral characteristics of the object and background, the subpixel edge locations are affected in some video frames; this resulted in differences in the amplitudes of both signals in those frames.

The frequency analysis results of the proposed method of area A and area B are shown in Fig. 18. Clearly, the peak of area A and area B coincide with each other. Besides, both areas have the same peak at 5 Hz, which is the same as the rotation speed of the cylindrical object in real data (i.e., 5 rps).

4. Conclusion

In this study, we proposed a method to detect the vibrations of a rotating cylindrical object. We used the frame magnification technique together with the subpixel-based edge detection technique to effectively detect the subpixel location of the edges of the rotating structure. Then, an edge tracking technique was introduced to track the edge locations in ROI around the rotating axis of the cylindrical structure and to remove the falsely detected edges from the ROI. The edge tracking technique uses the information of the edge location in the previous frame together with the current locations of an edge in the current pixel and in the next pixel. To perform the experiments, two simulation datasets were prepared by adding sinusoidal noises together with the random noise to the image of a

static cylindrical object, and a video of a real rotating cylindrical object was taken.

In the simulation datasets, we could qualitatively and quantitatively prove that the proposed method could effectively detect the vibrations on the rotating axis of a cylindrical structure with the exact locations of the edges while removing the non-interest edges or false edges. In the real dataset, we proved that the proposed method could detect the vibrations of a rotating structure regardless of the uneven background and brightness in a video. Also, unlike the existing vibration detection methods, the proposed method was not highly dependent on the ROI size because of applying the frame magnification step.

The proposed method can work on videos acquired by a commercially available camera of cylindrical rotating objects placed in dangerous areas or irradiated areas, e.g., rotation-based renewable power generation systems where surveyors cannot easily approach to a structure. Although we acquired a video of the rotating shaft with a close distance from the camera to the structure around 135 cm in this study, it can be further measured with a much longer distance. It is worth noting that the amplitude of the vibration signal to be detected by the proposed method depends on the distance between the camera and the rotating structure. If the distance between them increases the estimation of the vibration signal with minimum amplitude will proportionally decrease.

One of the advantages of the proposed method is that it can detect the vibration in multiple regions around the rotating structure at the same time. It can easily be carried out by selecting multiple ROIs where we are interested in and thus by measuring the vibration simultaneously. Moreover, because of the edge-based approach, the proposed method can detect not only the rotation-related vibrations but also the edge deformations or line-based cuts on a structure which can negatively affect the performance of a structure.

In our future work, we will focus on magnifying and removing small invisible motions (which can affect the vibration detection results) from the videos by using the proposed method with the motion magnification techniques. Furthermore, we will work on detecting the vibration in multiple dimensions by synchronizing two cameras and acquiring the videos from different directions. Also, the method will be tested on videos of remote rotating structures having different shapes.

Declaration of Competing Interest

The authors declare that they have no known competing financial interests or personal relationships that could have appeared to influence the work reported in this paper.

Acknowledgement

This work was supported by Korea Hydro & Nuclear power CO., LTD (No. 2019-TECH-13).

References

[1] J. Baqersad, P. Poozesh, C. Niezrecki, P. Avitabile, Photogrammetry and optical methods in structural dynamics–A review, Mech. Syst. Sig. Process. 86 (2017) 17–34.
[2] R. Burtch, History of photogrammetry: Notes of the Center for Photogrammetric Training, Ferris State University, USA, 2004.
[3] H.A. Beyer, Automated dimensional inspection with real-time photogrammetry, ISPRS J. Photogramm. Remote Sens. 50 (3) (1995) 20–26.
[4] T. Luhmann, Close range photogrammetry for industrial applications, ISPRS J. Photogramm. Remote Sens. 65 (6) (2010) 558–569.
[5] H.L. Mitchell, Applications of digital photogrammetry to medical investigations, ISPRS J. Photogramm. Remote Sens. 50 (3) (1995) 27–36.
[6] C.S. Fraser, K.L. Edmundson, Design and implementation of a computational processing system for off-line digital close-range photogrammetry, ISPRS J. Photogramm. Remote Sens. 55 (2) (2000) 94–104.
[7] D. Kalpoe, K. Khoshelham, B. Gorte, Vibration measurement of a model wind turbine using high speed photogrammetry, in: In Videometrics, Range Imaging, and Applications XI, International Society for Optics and Photonics, 2011, p. 80850J.
[8] M.A. Sutton, W.J. Wolters, W.H. Peters, W.F. Ranson, S.R. McNeill, Determination of displacements using an improved digital correlation method, Image Vis. Comput. 1 (3) (1983) 133–139.
[9] T.C. Chu, W.F. Ranson, M.A. Sutton, Applications of digital-image-correlation techniques to experimental mechanics, Exp. Mech. 25 (3) (1985) 232–244.
[10] U.P. Poudel, G. Fu, J. Ye, Structural damage detection using digital video imaging technique and wavelet transformation, J. Sound Vib. 286 (2005) 869–895.
[11] S. Patsias, W.J. Staszewskiy, Damage detection using optical measurements and wavelets, Structur. Health Monitor. 1 (1) (2002) 5–22.
[12] W. Wang, X. Li, Y. Ahmat, X. Hu, A. Chen, Vibration measurement method based on point tracking for irregular structures, Optik 176 (2019) 482–490.
[13] B. Gwashavanhu, A.J. Oberholster, P.S. Heyns, Rotating blade vibration analysis using photogrammetry and tracking laser Doppler vibrometry, Mech. Syst. Sig. Process. 76 (2016) 174–186.
[14] W. Wang, X. Li, A. Chen, A method of modal parameter identification for wind turbine blade based on binocular dynamic photogrammetry, Shock Vib. 2019 (2019) 1–10.
[15] C.C. Chang, Y.F. Ji, Flexible videogrammetric technique for three-dimensional structural vibration measurement, J. Eng. Mech. 133 (6) (2007) 656–664.
[16] P.F. Pai, D. Feng, Y. Duan, High-fidelity camera-based method for noncontact vibration testing of structures, in: In 54th AIAA/ASME/ASCE/AHS/ASC Structures, Structural Dynamics, and Materials Conference, 2013, p. 1898.
[17] A. Cigada, P. Mazzoleni, E. Zappa, M. Franzi, Cameras as displacement sensors to get the dynamic motion of a bridge: Performance evaluation against traditional approaches, in: In 6th International Conference on Bridge Maintenance, Safety and Management, 2012, pp. 2835–2841.
[18] A. Cigada, P. Mazzoleni, M. Tarabini, E. Zappa, Static and dynamic monitoring of bridges by means of vision-based measuring system, in: Topics in Dynamics of Bridges, Springer, New York, NY, 2013, pp. 83–92.
[19] L. Yu, B. Pan, Single-camera high-speed stereo-digital image correlation for full-field vibration measurement, Mech. Syst. Sig. Process. 94 (2017) 374–383.
[20] Y. Liu, H. Gao, J. Zhuge, J. Zhao, Research of under-sampling technique for digital image correlation in vibration measurement, in: Shock & Vibration, Aircraft/Aerospace, Energy Harvesting, Acoustics & Optics, Springer, Cham, 2017, pp. 49–58.
[21] R. Huňady, P. Pavelka, P. Lengvarský, Vibration and modal analysis of a rotating disc using high-speed 3D digital image correlation, Mech. Syst. Sig. Process. 121 (2019) 201–214.
[22] M. Cuadrado, J. Pernas-Sánchez, J.A. Artero-Guerrero, D. Varas, Model updating of uncertain parameters of carbon/epoxy composite plates using digital image correlation for full-field vibration measurement, Measurement 159 (2020) 107783, https://doi.org/10.1016/j.measurement.2020.107783.
[23] H. Nguyen, Z. Wang, P. Jones, B. Zhao, 3D shape, deformation, and vibration measurements using infrared Kinect sensors and digital image correlation, Appl. Opt. 56 (32) (2017) 9030–9037.
[24] Z. Chen, X. Zhang, S. Fatikow, 3D robust digital image correlation for vibration measurement, Appl. Opt. 55 (7) (2016) 1641–1648.
[25] Y.F. Ji, C.C. Chang, Nontarget image-based technique for small cable vibration measurement, J. Bridge Eng. 13 (2008) 34–42.

[26] A. Cigada, P. Mazzoleni, E. Zappa, Vibration monitoring of multiple bridge points by means of a unique vision-based measuring system, Exp. Mech. 54 (2014) 255–271.
[27] B. Shan, S. Zheng, J. Ou, Free vibration monitoring experiment of a stayed-cable model based on stereovision, Measurement 76 (2015) 228–239.
[28] D.T. Bartilson, K.T. Wieghaus, S. Hurlebaus, Target-less computer vision for traffic signal structure vibration studies, Mech. Syst. Sig. Process. 60 (2015) 571–582.
[29] K.S. Son, H.S. Jeon, G.S. Chae, J.S. Park, S.O. Kim, A fast high-resolution vibration measurement method based on vision technology for structures, Nuclear, Eng. Technol. (2020).
[30] R.C. Gonzalez, R.E. Woods, S.L. Eddins, Digital image processing using MATLAB, Pearson Education India, 2004.
[31] A. Cigada, M. Vanali, E. Zappa, Vision-based vibration monitoring of a large steel structure, in: Experimental Vibration Analysis for Civil Engineering Structures (EVACES), 2011, pp. 561–568.
[32] Y. Ji, C.C. Chang, Identification of structural dynamic behavior for continuous system based on videogrammetric technique. Smart Structures and Materials 2006: Smart Structures and Integrated Systems, International Society for Optics and Photonics, 2006.
[33] C. C. Chang, From photogrammetry, computer vision to structural response measurement, In Sensors and Smart Structures Technologies for Civil, Mechanical, and Aerospace Systems 2007, Vol. 6529, International Society for Optics and Photonics. 2007.
[34] K.S. Son, H.S. Jeon, J.H. Park, J.W. Park, Vibration displacement measurement technology for cylindrical structures using camera images, Nucl. Eng. Technol. 47 (2015) 488–499.
[35] A. Trujillo-Pino, K. Krissian, M. Alemán-Flores, D. Santana-Cedrés, Accurate subpixel edge location based on partial area effect, Image Vis. Comput. 31 (2013) 72–90.
[36] K. Sekar, V. Duraisamy, A.M. Remimol, An approach of image scaling using DWT and bicubic interpolation, in: In 2014 International Conference on Green Computing Communication and Electrical Engineering (ICGCCEE) IEEE, 2014, pp. 1–5.
[37] D.H. Lee, W.R. Lee, Easy measuring instrument for analyzing the radial and tilt error motions of a rotating shaft, Proc. Inst. Mech. Eng., Part M: J. Eng. Maritime Environ. 231 (2) (2017) 667–674.